Breaking waves: Bifurcations leading to a singular wave state

W. Tao Shi, Christopher L. Goodridge, and Daniel P. Lathrop*
Department of Physics, Emory University, Atlanta, Georgia 30322
(Received 23 September 1996)

We examine free surface wave singularities that show a violent focusing of energy. Periodic, modulated, and frequency locked wave states lead to a state with fluid spikes. When the excitation of free surface waves exceeds a well defined threshold, the waves break leading to a low-dimensional aperiodic state with spikes, droplet ejection, and air entrainment. Return maps formed from wave height measurements lead to a low-dimensional model of the dynamics. Surprisingly, only a slight increase in power dissipation is observed past the transition to ejecting waves. [S1063-651X(97)10909-6]

PACS number(s): 47.20.Ma, 47.55.Dz, 68.10.−m, 92.10.Hm

Recent observations of strongly forced standing waves have indicated a transition where wave breaking with spray and air entrainment occurs [1]. The simplest ejecting state observed shows a height $h \sim r^{-1/2}$ divergence on the free surface (for cylindrical coordinate r centered on the spike). An ultraviolet cutoff for these singularities is supplied by the Rayleigh instability [2], whereby the tip breaks up into droplets. Wave breaking states necessarily contain singularities, as they exhibit a change from a simply connected to a multiply connected free surface. Nonlinear spatiotemporal systems showing local singularities are often considered either high or infinite dimensional [3,4]. We present the sequence of bifurcations leading to ejecting states and the characterization of this dynamical system by analysis of the wave height time sequence and average power dissipation. Poincaré sections of the measured time series of wave height reveal a *low-dimensional* attractor of an unusual form: it has a divergence corresponding to the large amplitude peaks of the waves.

A straightforward laboratory system for observing these singularities and bifurcations involves vertically shaking a vessel that is partially filled with liquid. Parametrically forced surface waves were first studied experimentally in 1831 by Faraday [5]. Since then, the onset of periodic surface waves and the existence of spatial and temporal chaos in this system have been extensively studied, including the formation of quasicrystals and other wave phenomena [6–10]. Later theoretical and experimental observations have pointed to a transition leading to cusps and singularities when the surface changes topology [12,13]. Perhaps the first obervation of fluid jets produced by vertical oscillation were reported by Longuet-Higgins [11]. Other physical systems exhibiting local singularities have also been studied (nonlinear optical blowup and Euler systems) [14,15]. These past studies of singularities have not observed low-dimensional models for the global motion as we present here.

In our Faraday system, we mount a square Plexiglas tank, 12 cm on edge and 28 cm high to an electromagnetic linear actuator. This linear actuator is driven by a power amplifier following a sinusoidal signal from a signal generator. A linear air bearing is used to constrain the motion of the apparatus to be purely vertical. The tank is filled to a depth of 6.7 cm with a water-glycerin mixture [16], and shaken at a frequency of 7.4 Hz to excite a (2,2) Fourier mode. A highly viscous liquid is chosen here to dampen high wave number surface modes. Surface waves are influenced by meniscus effects [8] as well. The central region and the corner areas of the liquid surface oscillate out of phase. Large amplitude waves couple with the meniscus waves oscillating at the driving frequency. Thus the excited (2,2) mode is deformed in comparison to a linear mode with Neumann boundary conditions, and has a small additional time dependence at the driving frequency.

The sequence of bifurcations leading to breaking waves can be seen in the wave height and fluid power dissipation measurements for different wave states. When the acceleration amplitude of the tank is increased at the frequency $\omega/2\pi = 7.4$ Hz, the following sequence of states is observed: periodic waves with a frequency of $\omega/4\pi$, modulated waves, and ejecting singular waves. When the container is shaken off the 7.4 Hz resonance, hysteresis occurs in the onset of periodic waves. The acceleration amplitude of the excitation is measured by differentiating the measured displacement of the tank [17].

In order to analyze the observed transitions, a new laser diagnostic technique was devised to measure the surface wave height. The technique utilizes a vertical laser sheet, 1 mm wide by 11 cm high, which propagates horizontally across the wave tank through its center. The bottom of the laser sheet is aligned to coincide with the flat liquid surface at rest. When the tank is oscillated, the laser sheet scatters off the curved surface of the excited waves. Those portions of the sheet above the maximum wave height propagate unscattered. The unscattered light is collected by a parabolic mirror and then focused onto a photodiode to measure the amplitude of the light. The photodiode signal is then digitized to obtain a time series of wave height. With a uniform intensity profile, the light amplitude falling on the photodiode is proportional to the sheet height above the waves. This technique yields a time series of the maximum wave height across one cross section of the apparatus. The uniformity of the laser sheet is accomplished by overexpanding the beam and using only the central portion. The laser light is stabilized with an optoacoustic modulator and feedback from the light-controlled beam. The error of the wave height measurements is estimated to be 2.5%.

*Electronic address: dpl@complex.physics.emory.edu

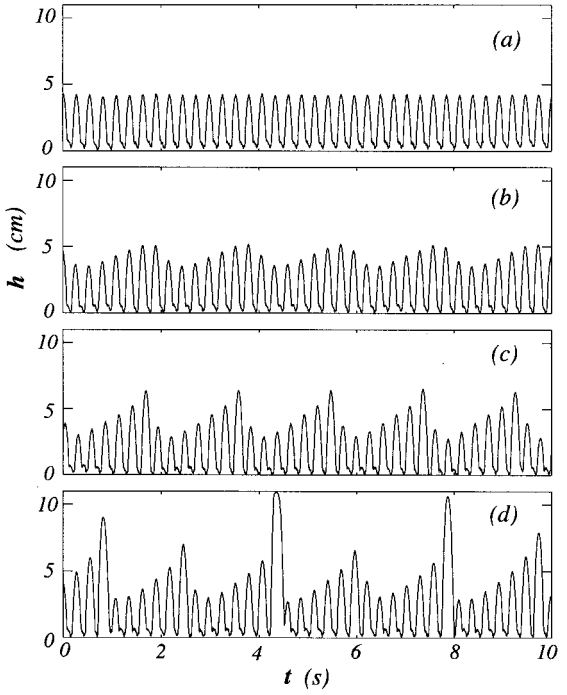

FIG. 1. Time series of the wave height at a driving frequency of 7.4 Hz near the modulation threshold: (a) a periodic state (4.72 m/s^2), (b) a modulated state (4.98 m/s^2), (c) a period-7 state (5.08 m/s^2), and (d) an ejecting state (5.16 m/s^2). The flattened top of the peak at $t=4.32$ s in (d) indicates that the height of the ejecting wave has exceeded the range of the diagnostic optics. The height of the ejecting wave state is no longer periodic and varies with each ejecting event.

Figure 1 shows four examples of the wave height measurements, including a state where the excited surface waves become severely modulated and start to form spikes and entrain bubbles every 6 or 7 basic periods [Fig. 1(d)].

From the measurements of the wave height, we construct a diagram of the frequencies involved in the wave motion from power spectra of the wave height (Fig. 2). The map shows the transitions leading from the tranquil surface to surface wave states. A number of bifurcations can be seen as the applied forcing is increased. Periodic waves are first visible at 3.86 m/s^2. These waves evolve into quasiperiodic states at 4.96 m/s^2, to period-7 states at 5.06 m/s^2, then to broadband ejecting states at 5.10 m/s^2, and finally to period-6 states at 5.28 m/s^2, with other periodic windows also visible. Very low noise levels in quasiperiodic and multiply periodic states produce the blue background in the map. The spectra of the ejecting states have greater background noise (the yellow background in the map) implying aperiodic motion. Above 5.80 m/s^2, the waves show some swirling motion while ejecting.

To better understand the dynamics of the ejecting state, we construct a two-dimensional phase diagram $\{H_n, H_{n+1}\}$ from the maximum height H_n of each wave from the wave forms illustrated in Fig. 1; these return maps are shown in Fig. 3. The return map for the data in Fig. 1(a) reduces to a fixed point. Figure 3(a) shows a return map at $a=4.98$ m/s^2 displaying quasiperiodic motion. This limit cycle deforms as the acceleration is increased, shows a region of locked period-7 behavior [Fig. 3(b)] finally deforming and forming folds for the ejecting state [Fig. 3(c)]. This return map has developed a region of large amplitude excursions (here chopped above 11 cm due to limited height of the laser sheet). Thus waves with a maximum about 5.8 cm will be followed by a very large amplitude spike. This divergence in the return map corresponds to the filament tipped spikes observed in the experiment. These spikes are routinely observed hitting the lid of the container (25 cm above the flat surface level). These filament tipped waves have a height in excess of 1 m in other containers without lids.

A simple low-dimensional model of the return map can be used to describe the height of the ejecting waves:

$$H_{n+1}=\begin{cases}\gamma H_n+\dfrac{0.040H_n}{(H_n-0.48\lambda)^2}, & H_n<0.48\lambda \\ 2.8+\dfrac{0.14H_n}{(H_n-0.48\lambda)^2}, & H_n>0.48\lambda,\end{cases} \tag{1}$$

where λ is the wavelength of the waves ($\lambda=12$ cm here) and γ a constant varying from 1 to 1.5 [$\gamma=1.19$ for Fig. 3(c)]. This low-dimensional model shows periodic windows comparable to the experimentally observed sequence. The location for the pole, at $H_n=0.48\lambda$, is approximately independent of acceleration in the ejecting states, and is likely a consequence of geometry alone. The model includes a linear growth term (γH_n) for small amplitude waves, and a mechanism for large amplitude ejections and reentrainment. This map does not capture the observed quasiperiodic to ejecting chaotic transition. A mapping involving H_{n-1} would better serve to model this earlier transition.

We have also measured the power loss due to the dissipation of the liquid flow in order to further investigate the transition among wave states. This was done in anticipation of a large power dissipation increase at the transition to ejecting waves. We measure the power by simultaneously monitoring the global force transmitted to the tank and the instantaneous velocity of the tank. The product of these two quantities yields the instantaneous power flux. The driving force is measured using a strain gauge mounted to the tank. The instantaneous velocity is determined by differentiating the instantaneous vertical position of the tank [17]. In order to account for power dissipated by the mechanical components (i.e., air bearings) of the system, power measurements were taken with the tank empty of fluid but containing an equivalent amount of weight. This zero point dissipation was subtracted from all future measurements. Although the forcing is sinusoidal, the reaction forces due to liquid flow cause the small additional motions that reflect the wave state (typically 1% of the large sinusoidal motion). The time average of the power due to these small additional motions is estimated to be 10^{-6} smaller than those due to the fundamental frequency. Therefore, the averaged power dissipation is approximately due to only the force and velocity components at the driving frequency:

$$P=\tfrac{1}{2}\omega D_A F_A \sin(\phi_F-\phi_D), \tag{2}$$

where D_A and F_A are the amplitude of displacement and the amplitude of force at the driving frequency $\omega/2\pi$. The av-

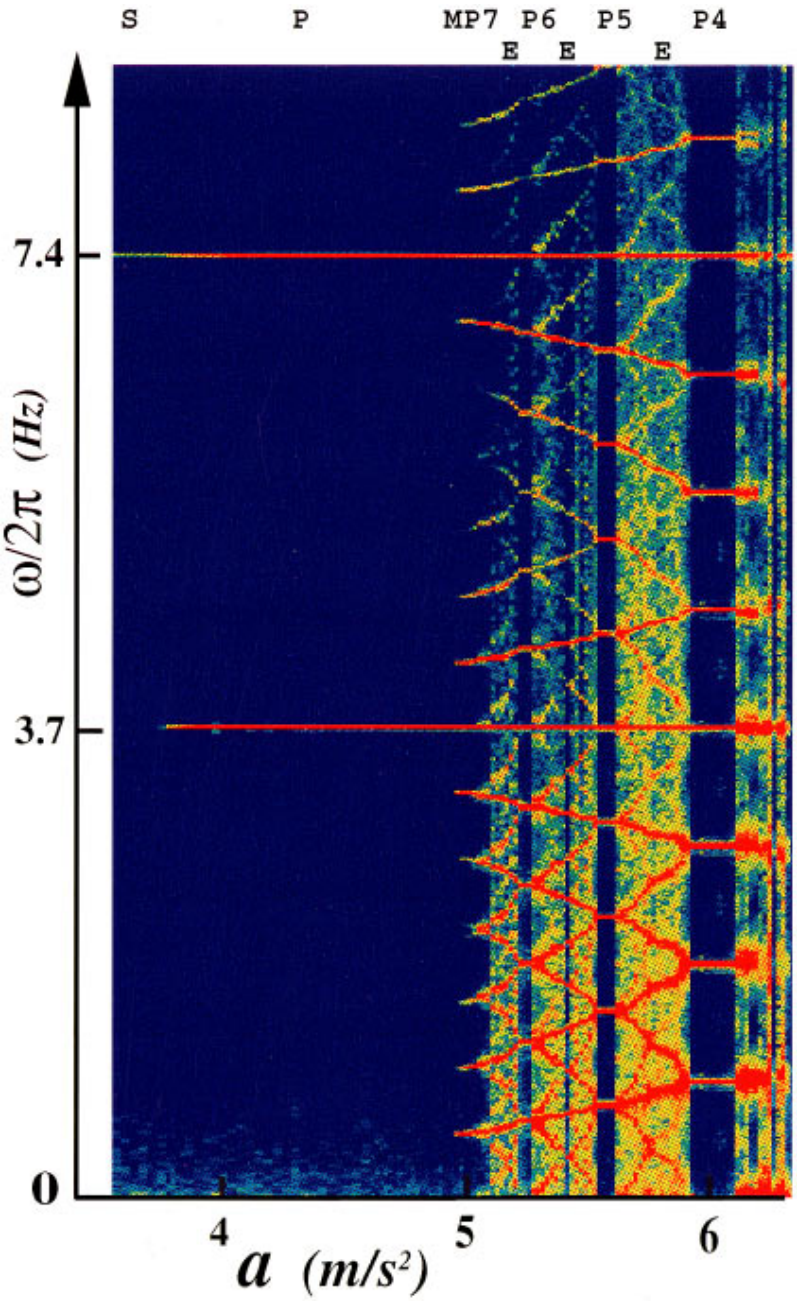

FIG. 2. (Color). A map of the power spectrum of wave height as a function of the excitation acceleration and the spectrum frequency, all with forcing frequency 7.4 Hz. Color represents the amplitude of the spectrum components, scaled from blue to red. Each vertical strip represents one power spectrum as measured at a particular peak amplitude of acceleration of the tank a_c. Letters above denote stationary S, periodic P, modulated M, period-n Pn, and ejecting E wave states.

eraged dissipation is thus determined by the phase delay $\phi_F - \phi_D$ between the driving force, and the displacement at the driving frequency. The phase is measured using fast Fourier transforms of the digitized position and force signals. The errors in the measurements of displacement, force and phase are estimated to be 2%, 2.5%, and 6%, respectively.

We have measured the variation of the power dissipation with increasing acceleration at several frequencies. The measured power dissipation as a function of the excitation acceleration at 7.4 Hz is shown in Fig. 4(b). The other curves off resonance (7.2 and 7.0 Hz) show similar trends except for substantial hysteresis. Each point in Fig. 4(b) represents an average over 5 min. For comparison, we also plot the maximum wave height as a function of the acceleration [Fig. 4(a)]. The averaged power dissipation is zero in the tranquil state and then increases with the excitation acceleration after the onset of the simple subharmonic waves at 3.86 m/s^2. The averaged power dissipation increases slightly, but fails to show a dramatic increase with the onset of the singularities (5.10 m/s^2). From this we can conclude that the surface spikes are only a minor factor in the overall system dissipation.

The power dissipation of a simple periodic wave state can be estimated from considerations of linear growth and decay rate. We follow Cross and Hohenberg [19] in defining a decay rate α of a surface wave. This constant can be extracted from measurements of the initial growth rate, as a function of the driving acceleration. Cross and Hohenberg estimate the initial exponential growth rate as

$$\beta = -\alpha + \sqrt{(\kappa a)^2 - (\omega - \omega_0)^2}, \tag{3}$$

where ω_0 is the resonant angular frequency for the (2,2) mode, and a is the excitation acceleration amplitude. The

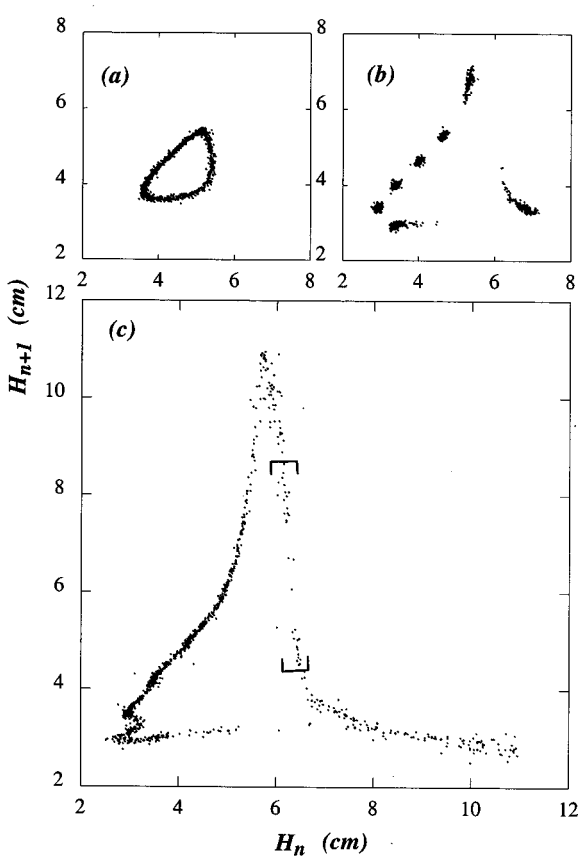

FIG. 3. Return maps showing (a) quasiperiodic motion, (b) period-7 motion, and (c) an aperiodic ejecting state formed from local maximum values H_n from time series shown in Fig. 1. Note that the instrument saturates at 11 cm and waves are observed in (c) with filaments which hit the roof of the container (28 cm high). Those points between the two square brackets in Fig. 3(c) show entrainment and oscillations of air bubbles below the surface [18].

coefficients α and κ are found from a fit to the experimental data of the growth of waves from a sudden start: $\alpha = 2.75\ \mathrm{s}^{-1}$ and $\kappa = 0.70$ s/m at the driving frequencies $\omega/2\pi = 7.2$ and 7.4 Hz. The estimated dissipation can be calculated as

$$P_e = E[1 - \exp(-2\alpha T)]/T, \tag{4}$$

where E and T are the total energy and the period of the basic periodic wave. The total energy is taken as the gravitational potential energy of the wave at its maximum height, and is calculated from an side view image of the state. The estimate for the power dissipation is then 16 mW for an acceleration of 4.62 $\mathrm{m/s}^2$, which is in reasonable agreement with the measurement (20 mW) given in Fig. 4(b) at the similar excitation. This estimate in turn confirms our power measurements, and the interpretation that the dissipation is due largely to the smooth wave motions and not the singularities.

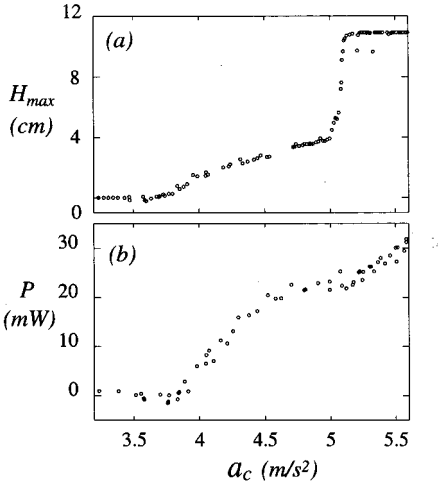

FIG. 4. (a) Time-averaged power dissipation and (b) maximum wave height as a function of the excitation acceleration at a driving frequency of 7.4 Hz. The flat top in Fig. 4(b) indicates that the heights of the ejecting wave saturated the diagnostic optics.

Measurements of wave height and power dissipation show a sequence of bifurcations leading to a state that has large amplitude peaks and droplet ejections. Low-dimensional behavior is still evident in the singular wave state. A return map of maximum wave height develops a pole that causes ejections following waves with a critical wave height. Details of the mechanism for the focusing of kinetic energy producing the spikes are left to a future paper.

We would like to acknowledge helpful discussions with R. Behringer, M. Brenner, H. G. E. Hentschel, S. E. Ralph, R. Roy, and H.L. Swinney. This work was partially supported by the Emory University Research Committee.

[1] C. L. Goodridge, W. T. Shi, and D. P. Lathrop, Phys. Rev. Lett. **76**, 1824 (1996).
[2] S. Chandrasekhar, *Hydrodynamic and Hydromagnetic Stability* (Dover Publications, Inc., New York, 1981).
[3] M. Bartuccelli, P. Constantin, C. R. Doering, J. D. Gibbon, and M. Gisselfalt, Phys. Lett. A **142**, 349 (1989).
[4] M. Bartuccelli, P. Constantin, C. R. Doering, J. D. Gibbon, and M. Gisselfalt, Physica D **44**, 421 (1990).
[5] M. Faraday, Philos. Trans. R. Soc. London **121**, 299 (1831).
[6] T. B. Benjamin and F. Ursell, Proc. R. Soc. London, Ser. A **225**, 505 (1954).
[7] R. Keolian, L. A. Turkevich, S. J. Putterman, and I. Rudnick, Phys. Rev. Lett. **47**, 1133 (1981); J. P. Gollub and C. W. Meyer, Physica D **6**, 337 (1983).
[8] S. Douady, J. Fluid Mech. **221**, 383 (1990); J. Miles and D. Henderson, Annu. Rev. Fluid Mech. **22**, 143 (1990).
[9] W. S. Edwards and S. Fauve, Phys. Rev. E **47**, R788 (1993); N. B. Tufillaro, R. Ramshankar, and J. P. Gollub, Phys. Rev. Lett. **62**, 422 (1989).
[10] S. Cilberto, S. Douady, and S. Fauve, Europhys. Lett. **15**, 23 (1991); O. N. Mesquita, S. Kane, and J. P. Gollub, Phys. Rev. A **45**, 3700 (1992).

[11] M. S. Longuet-Higgins, J. Fluid Mech. **127**, 103 (1983).
[12] A. C. Newell and V. E. Zakharov, Phys. Rev. Lett. **69**, 1149 (1992).
[13] E. A. Kuznetsov, M. D. Spector, V. E. Zakharov, Phys. Rev. E **49**, 1283 (1994).
[14] Y. R. Shen, *The Principles of Nonlinear Optics* (John Wiley and Sons, Inc., New York, 1984).
[15] S. Balachandar and R. Mittal, Bull. Am. Phys. Soc. **40**, 1996 (1995).
[16] The tank was filled with 960 ml of a 92% glycerin and 8% distilled water solution with $\nu=2.86$ cm^2/s.
[17] The instantaneous vertical displacement of the tank is measured using a linear potentiometer. The errors in the determination of the acceleration amplitude are about 2%.
[18] A piezoelectric transducer was attached to the tank side wall for the purpose of detecting air bubble oscillations.
[19] M. C. Cross and P. C. Hohenberg, Rev. Mod. Phys. **65**, 851 (1993).